HHS Public Access

Author manuscript

Cell. Author manuscript; available in PMC 2016 June 18.

Published in final edited form as:

Cell. 2015 June 18; 161(7): 1576–1591. doi:10.1016/j.cell.2015.05.029.

Glucose uptake and Runx2 synergize to orchestrate osteoblast differentiation and bone formation

Jianwen Wei[#1], **Junko Shimazu**[#1], **Munevver P. Makinistoglu**[1], **Antonio Maurizi**[1], **Daisuke Kajimura**[1], **Haihong Zong**[2], **Takeshi Takarada**[3], **Takashi Iezaki**[3], **Jeffrey E. Pessin**[2], **Eiichi Hinoi**[3], and **Gerard Karsenty**[1,*]

[1] Department of Genetics & Development, College of Physicians and Surgeons, Columbia University, New York, NY 10032, USA

[2] Department of Medicine and Molecular Pharmacology, The Albert Einstein College of Medicine, Bronx, New York, NY 10461, USA

[3] Laboratory of Molecular Pharmacology, Faculty of Pharmacy, Institute of Medical, Pharmaceutical and Health Sciences, Kanazawa University, Kanazawa, Ishikawa 920-1192, Japan.

[#] These authors contributed equally to this work.

Summary

The synthesis of Type I collagen, the main component of the bone matrix, precedes the expression of *Runx2*, the earliest determinant of osteoblast differentiation. We hypothesized that the osteoblast's energetic needs might explain this apparent paradox. We show here that glucose, the main nutrient of osteoblasts, is transported in these cells through *Glut1* whose expression precedes that of *Runx2*. Glucose uptake favors osteoblast differentiation by suppressing the AMPK-dependent proteasomal degradation of Runx2 and promotes bone formation by inhibiting another function of AMPK. While Runx2 cannot induce osteoblast differentiation when glucose uptake is compromised, raising blood glucose levels restores collagen synthesis in *Runx2*-null osteoblasts and initiates bone formation in *Runx2*-deficient embryos. Moreover, Runx2 favors *Glut1* expression, and this feed-forward regulation between Runx2 and *Glut1* determines the onset of osteoblast differentiation during development and the extent of bone formation throughout life. These results reveal an unexpected intricacy between bone and glucose metabolism.

[*]Address correspondence to: Gerard Karsenty, Department of Genetics and Development, 701W 168th Street, Room 1602A HHSC, New York, New York 10032, USA. Phone: 212.305.4011; Fax: 212.923.2090; gk2172@columbia.edu..

Conflict of interest: The authors have no conflict of interest to declare.

Author Contributions

J.W. and G.K. conceived and designed the studies; J.W. and J.S. performed most experiments; M.M generated the *Glut1fl/fl* mice; A.M. performed some histological analysis; D.K. performed the in vivo AICAR treatment experiment; H.Z. and J.P. performed glucose clamp analyses; T.T., T.L. and E.H. performed experiments using *Runx2*−/− osteoblasts; J.W. and G.K. wrote the paper.

Introduction

The transcription factor Runx2 is a master determinant of osteoblast differentiation (Long, 2012; Karsenty et al., 2009). Its expression in prospective osteoblasts precedes osteoblast differentiation, its inactivation prevents osteoblast differentiation and its haplo-insufficiency causes a skeletal dysplasia called cleidocranial dysplasia (CCD) that is characterized by a delay in osteoblast differentiation leading to hypoplastic clavicles and open fontanelles. Several aspects of Runx2 biology remain however poorly understood. For example, the nature of the molecular events leading to Runx2 accumulation in cells of the osteoblast lineage is largely unknown. A second question is to determine if and how Runx2 contributes to bone formation by differentiated osteoblasts. A peculiar feature of osteoblast biology raises this latter issue.

Type I collagen is by far the most abundant protein of the bone extracellular matrix (ECM) and its synthesis by osteoblasts is often considered a biomarker of bone formation. Type I collagen is a heterotrimeric protein made of two α1(I) chains and one α2(I) chain that are encoded by two different genes (Vuorio and de Crombrugghe, 1990). In vitro, Runx2 can bind to and up-regulate the activity of a *α1(I) Collagen* promoter fragment (Kern et al., 2001). In vivo, however, Type I collagen synthesis precedes *Runx2* expression in prospective osteoblasts. Thus, the regulation of Type I collagen synthesis in osteoblasts is not fully understood, and by extension since the bone ECM is mainly made of Type I collagen, it is also unclear how bone formation by osteoblasts is regulated.

Besides being responsible of bone formation, the osteoblast is an endocrine cell that secretes a hormone, osteocalcin that favors glucose homeostasis (Lee et al., 2007). Notwithstanding the molecular complexity of this emerging regulation, the identification of bone as a regulator of glucose metabolism raises a fundamental question: why would bone have this role? A prerequisite to answering this question is to define the functions of glucose in osteoblasts.

Here we asked if the energetic needs of the osteoblast might explain how osteoblast differentiation and bone formation occurs in vivo. We found that glucose is the main nutrient of osteoblasts and it is transported in these cells in an insulin-independent manner through the facilitative *Glut1* glucose transporter whose expression precedes that of *Runx2* during skeletogenesis. By inhibiting one activity of AMPK, glucose is necessary for Runx2 accumulation and osteoblast differentiation; through the inhibition of another AMPK function glucose is necessary for collagen synthesis and bone formation. Moreover, by promoting Runx2 accumulation, glucose uptake in osteoblasts favors *Osteocalcin* expression and whole-body glucose homeostasis. We further show that Runx2 is not sufficient for timely osteoblast differentiation and proper bone formation if glucose uptake is compromised whereas raising blood glucose levels induces collagen synthesis and bone formation in the absence of *Runx2*. The relationship between Runx2 and glucose uptake is even more elaborate since Runx2 is needed for *Glut1* expression in osteoblasts. This crosstalk between Runx2 and glucose uptake acts as an amplification mechanism allowing osteoblast differentiation and bone formation to be coordinated throughout life. This study

provides a bone-centric illustration of the importance of the crosstalk between bone and glucose metabolism.

Results

Insulin-independent glucose uptake in osteoblasts

To determine what is/are the main nutrient(s) used by osteoblasts we measured their oxygen consumption rate (OCR) when incubated with individual nutrients. Like neurons and unlike myoblasts, osteoblasts had the highest OCR when cultured in the presence of glucose and the lowest when cultured in the presence of a representative fatty acid (Figure 1A). These results prompted us to measure through euglycemic hyperinsulinemic clamps the amount of glucose taken up by bone and the mechanism whereby it occurs in 3 month-old wild-type (WT) mice.

In the conditions of this assay bone takes up a fifth of the quantity of glucose taken up by skeletal muscle, the organ taking up the majority of glucose in the mouse (Ferrannini et al., 1988), and half of what is taken up by white adipose tissue (WAT) (Figure 1B). Unlike what is the case for skeletal muscle and WAT, glucose uptake in bone is not enhanced by insulin (Figure 1B). We also compared the uptake of 2-[U-^{14}C] deoxyglucose (2-DG) in osteoblasts and osteoclasts, to the one in myoblasts. Both bone cell types take up approximately a third of the quantity of 2-DG taken up by myoblasts and do so in an insulin-independent manner (Figure 1C). Consistent with these observations, *Glut1* that transports glucose in an insulin-independent manner, is expressed two orders of magnitude higher than any other class I glucose transporters in bone cells (Figure 1D). The rest of this study focuses on the functions of glucose in osteoblasts.

To establish the biological importance of *Glut1* expression in these cells, we analyzed osteoblasts lacking or over-expressing modestly (1.75 fold) *Glut1* (Figure S1A-B). *Glut1−/−* osteoblasts took up 75% less and *α1(I)Col-Glut1* osteoblasts 20% more 2-DG than control osteoblasts (Figure 1E). Consequently, glycogen content was decreased 50% in *Glut1−/−* and increased 40% in *α1(I)Col-Glut1* osteoblasts compared to control ones (Figure S1C). Thus Glut1 is responsible for the majority of glucose uptake in osteoblasts.

Glucose uptake is necessary for osteoblast differentiation during development

Next we analyzed *Glut1's* spatial and temporal pattern of expression during skeletogenesis by in situ hybridization and compared it to that of *α1(I) collagen* and *Runx2*, two marker genes of mesenchymal cells and osteoblasts; of *α1(II) Collagen*, a marker of non–hypertrophic chondrocytes; and of *α1(X) collagen* a marker of hypertrophic chondrocytes.

At E10.5 *Glut1* is highly expressed in *α1(I) Collagen*-expressing mesenchymal cells of the developing hindlimbs (Figure 1F panels a-j). *Runx2* begins to be expressed in *α1(I) Collagen/Glut1*-expressing cells at E12.5 and remains expressed in these cells throughout development (Figure 1F, panels k-o). Prior to E12.5 another *Runx* gene, *Runx1*, is expressed in *α1(I) Collagen/Glut1*-expressing cells (Figure 1F, panels p-t). The third *Runx* gene, *Runx3* is not expressed before E13.5 and its expression is predominant in *α1(II) Collagen*-expressing chondrocytes (Figure 1F, panels u-y, z-b1). *Glut1* is virtually not expressed in

chondrocytes (Figure 1F, panels a-e and z-e1). In view of this pattern of expression, we analyzed the function of *Glut1* during osteoblast differentiation by crossing mice harboring a floxed allele of *Glut1* (Figure S2A) with mice expressing the *Cre* recombinase under the control of *Dermo1* (Yu et al., 2003) ($Glut1_{dermo1}{}^{-/-}$) that delete genes starting at E12.5, or of *Osterix* regulatory elements (Rodda and McMahon, 2006) ($Glut1_{osx}{}^{-/-}$) that delete genes starting at E14.5. We verified in each case that *Glut1* was efficiently deleted in the targeted cells but not in other cell types or tissues and that expression of other *Gluts* was not affected by the *Glut1* deletion (Figure S2B-E).

Using alcian blue/alizarin red staining of skeletal preparations to distinguish nonmineralized (blue) from mineralized ECM (red), $Glut1_{dermo1}{}^{-/-}$ and control embryos were indistinguishable until E13.5 (Figure S2F). E14.0 was the first time point when a delay in ECM mineralization in long bones and the jaws was seen in $Glut1_{dermo1}{}^{-/-}$ embryos (Figure 2A). This difference in ECM mineralization between control and $Glut1_{dermo1}{}^{-/-}$ embryos was verified histologically (Figure 2B). At E14.5 ECM mineralization was still absent in the mandibles of $Glut1_{dermo1}{}^{-/-}$ embryos (Figure 2A). Beyond E14.5 we also studied $Glut1_{osx}{}^{-/-}$ embryos. At E15.5 large area of mineralized ECM were present in the axial skeleton of controls but not of $Glut1_{osx}{}^{-/-}$ and $Glut1_{dermo1}{}^{-/-}$ embryos except in long bones (Figure 2C, S2F). Von Kossa staining of histological sections detected extensive ECM mineralization in skeletal elements of control embryos, while this mineralization was more restricted in $Glut1_{osx}{}^{-/-}$ embryos; alcian blue staining of these sections showed that the ECM in $Glut1_{osx}{}^{-/-}$ skeletal elements was mostly of cartilaginous nature (Figure 2D). Consistent with this observation, *α1(X) Collagen*-expressing hypertrophic chondrocytes covered a larger area in $Glut1_{osx}{}^{-/-}$ than in control skeletal elements and expression of *Osteocalcin*, was undetectable in $Glut1_{osx}{}^{-/-}$ skeletal elements (Figure 2E) indicating that osteoblast differentiation was delayed in E15.5 $Glut1_{osx}{}^{-/-}$ embryos. Remarkably, despite these delays in osteoblast differentiation and bone formation, *Runx2* and *α1(I) Collagen* were normally expressed in E15.5 $Glut1_{osx}{}^{-/-}$ skeletal elements (Figure 2E).

At E18.5, the skull of $Glut1_{osx}{}^{-/-}$ embryos that ossifies mostly through an intramembranous process was poorly mineralized suggesting that osteoblast differentiation was delayed (Figure 2F). Von Kossa staining of histological sections showed numerous, long, and thick trabeculae in controls but not in $Glut1_{osx}{}^{-/-}$ long bones and an alcian blue staining showed many more cartilaginous remnants in $Glut1_{osx}{}^{-/-}$ than in control skeletal elements (Figure 2G). Accordingly, the area occupied by *α1(X) Collagen*-expressing hypertrophic chondrocytes remained larger in $Glut1_{osx}{}^{-/-}$ than in control skeletal elements and expression of *Osteocalcin* was still barely detectable (Figure 2H-J). This incomplete osteoblast differentiation in $Glut1_{osx}{}^{-/-}$ bones and osteoblasts was further illustrated by the decreased expression of *Bsp* (Figure 2I-J). This delay in osteoblast differentiation explains why E18.5 $Glut1_{osx}{}^{-/-}$ embryos had open fontanelles and hypoplastic clavicles (Figure 2F). Even though these two features are characteristic of CCD, a disease caused by a decrease in the function of Runx2 (Mundlos et al., 1997; Lee et al., 1997), *Runx2* expression was normal in E18.5 $Glut1_{osx}{}^{-/-}$ bones. The same was true for *α1(I) Collagen* expression (Figure 2H-J).

Accounting for this delay in osteoblast differentiation and CCD phenotype, there was a 70% decrease in Runx2 accumulation in E18.5 *Glut1*$_{osx}$*−/−* bones and osteoblasts (Figure 2K). This decrease in Runx2 accumulation was not observed for other transcription factors (Figure S2G). There was also a 70% decrease in Type I collagen accumulation in E18.5 *Glut1−/−* bones and osteoblasts because of a 60% decrease in the rate of collagen synthesis in *Glut1−/−* compared to control osteoblasts (Figure 2K-L). This latter finding explained the decreased bone formation in *Glut1*$_{osx}$*−/−* embryos. Of note, *Chrebp*, a transcriptional mediator of glucose signaling in other cell types (Yamashita et al., 2001), is not expressed and does not regulate glucose uptake in osteoblasts (Figure S2H-K).

Glucose uptake in osteoblasts is necessary for bone formation and whole-body glucose homeostasis post-natally

To study *Glut1* functions in osteoblasts post-natally, we crossed *Glut1fl/fl* mice with *Osteocalcin-Cre* mice (*Glut1*$_{ocn}$*−/−*) that do not initiate gene deletion before E18.5 (Zhang et al., 2002) and performed an inducible deletion of *Glut1* in osteoblasts in 6 week-old *Osx-Cre;Glut1fl/fl* mice (*Glut1*$_{Dox}$*−/−*). After verifying the specificity and efficiency of the gene deletions (Figure S3A-B), we examined both models of *Glut1−/−* mice at 3 months of age and included in this analysis *α1(I)Col-Glut1* mice that overexpress modestly (1.75-fold) *Glut1* in osteoblasts (Figure S2D).

Glut1$_{ocn}$*−/−* and *Glut1*$_{Dox}$*−/−* mice of either sex presented with a low bone mass in all bones analyzed whereas *α1(I)Col-Glut1* mice displayed a high bone mass. In these mouse models, only parameters of bone formation i.e., circulating levels of PINP, mineral apposition rate, bone formation rate and osteoblasts number were affected (Figure 3A-C, S3C-E). Expression of the cell cycle regulators *Ccnd2*, *Ccne1* and *Cdk4*, and osteoblast proliferation as measured by BrdU incorporation were decreased in *Glut1*$_{ocn}$*−/−* and increased in *α1(I)Col-Glut1* bones (Figure 3D-E). Again the accumulation not the expression, of Runx2 and Type I collagen was decreased in *Glut1*$_{ocn}$*−/−* and increased in *α1(I)Col-Glut1* bones (Figure 3F-G).

Following the fluctuation of Runx2 accumulation, expression of *Osteocalcin*, a Runx2 target gene, and circulating osteocalcin levels were low in *Glut1*$_{ocn}$*−/−* mice and high in *α1(I)Col-Glut1* compared to control mice (Figure 3F, S3F). As a result, insulin secretion after glucose stimulation, glucose tolerance measured by a glucose tolerance test, insulin sensitivity assessed by an insulin tolerance test and the steady-state glucose infusion rate during euglycemic-hyerpinsulinemic clamp, were suppressed in *Glut1*$_{ocn}$*−/−* mice and improved in *α1(I)Col-Glut1* compared to control mice (Figure 3H-N). In summary, glucose uptake in cells of the osteoblast lineage is necessary for osteoblast differentiation, bone formation, and whole-body glucose homeostasis.

Glucose uptake favors osteoblast differentiation and bone formation by inhibiting AMPK

To determine if the delay in osteoblast differentiation and the decrease in bone formation seen in *Glut1*$_{osx}$*−/−* embryos and mice were due to a decrease in protein synthesis that a poor glucose uptake triggers (Jeyapalan et al., 2007; Mayer et al., 2011), we measured AMP, ADP and ATP contents in *Glut1−/−* osteoblasts.

Although AMP and ATP levels were not affected, there was a 3-fold increase in ADP content leading to a 3-fold increase in the ratio of ADP over ATP in *Glut1*−/− versus control osteoblasts (Figure 4A, S4A). As a result, AMPK activity assessed by the phosphorylation of its α subunit at Thr172 and of its substrate ACC1 at Ser79 (Woods et al., 1994; Wilson et al., 1996) was increased (Figure 4B). Several lines of evidence indicated that the activity of the mTORC1 complex was decreased in *Glut1*−/− osteoblasts. Phosphorylation of the mTORC1 substrates p70S6K at Thr389, 4E-BP1 at Thr37 and eIF4G at Ser1108, was decreased (Bolster et al., 2002; Reiter et al., 2005) (Figure 4C), Raptor phosphorylation at Ser792 was increased and mTORC1 kinase activity was decreased in *Glut1*−/− osteoblasts (Figure 4B, D). Conversely, p70S6K phosphorylation and collagen accumulation were both decreased in *Raptor*−/− osteoblasts and knockdown of *Tsc1* and *Tsc2* not only restored mTORC1 activity as measured by p70S6K phosphorylation but also normalized collagen accumulation in *Glut1*−/− osteoblasts (Figure 4E, F).

To demonstrate that the decrease in mTORC1 activity and the phenotypes of the $Glut1_{osx}$−/− mice are caused by an increase in AMPK activity in osteoblasts we decreased the expression of *Ampk* in osteoblasts by generating *Glut1*−/− embryos or mice lacking in osteoblasts one allele of *Ampkchk1*, the most highly expressed AMPKα subunit in these cells (Figure 4G). Phosphorylation of AMPKα1 and p70S6K, ATP contents, Runx2 and Type I collagen accumulations were similar in $Glut1_{osx}$−/−;$Ampka1_{osx}$+/− and control osteoblasts indicating that AMPK activity and therefore mTORC1 signaling had been restored in $Glut1_{osx}$−/−;$Ampka1_{osx}$+/− osteoblasts (Figure 4H, S4B-C). As a result, alcian blue/alizarin red staining of skeletal preparations, histological and in situ hybridization analyses showed normal osteoblast differentiation and no evidence of CCD in $Glut1_{osx}$−/−;$Ampka1_{osx}$+/− embryos (Figure 4I-L). Bone formation parameters were also normal in $Glut1_{ocn}$−/−;$Ampka1_{ocn}$+/− mice (Figure 4M).

Two experiments showed that increasing AMPK activity in osteoblasts is deleterious for bone. Treating mouse osteoblasts with AICAR, an AMPK agonist, profoundly decreased Type I collagen and Runx2 accumulations in these cells and, WT mice treated with AICAR from 6 to 14 weeks of age showed a significant decrease in bone formation parameters and bone mass (Figure 4N-O). Accordingly and as it is the case for *Glut1*−/− osteoblasts, WT osteoblasts deprived of glucose had higher levels of P-AMPK and lower levels of P-P70S6K and type I collagen than if cultured in the presence of glucose (Figure S4D).

Runx2 cannot induce osteoblast differentiation when glucose uptake is hampered

In the course of these experiments, we noticed that Runx2 accumulation was restored when *Glut1*−/− osteoblasts were treated with an inhibitor of proteasome degradation and that Runx2 ubiquitination was increased in *Glut1*−/− osteoblasts (Figure 5A). That Runx2 ubiquitination is normal in *Glut1*−/−;*Ampka1*+/− and *Glut1*−/−;*Ampka1*−/− osteoblasts (Figure 5B) implicated AMPK in Runx2 polyubiquitination. Mass spectrometry and bioinformatics analyses identified a possible AMPK recognition site in Smurf1, an E3 ubiquitin ligase involved in Runx2 degradation (Zhao et al., 2003) (Figure S5A-B). In vitro, AMPK phosphorylated Smurf1 at Ser148 and this phosphorylation event was needed for Smurf1-induced Runx2 ubiquitination (Figure 5C-D). Smurf1 phosphorylation at Ser148 did

not increase in *Ampka1−/−* osteoblasts and Runx2 accumulation did not decrease in *Ampka1−/−* or *Smurf1−/−* osteoblasts cultured in the absence of glucose as it did in WT osteoblasts (Figure 5E-F). Moreover, an anti-phospho-Smurf1 antibody demonstrated AMPKα1 interaction with phospho-Smurf1 in *Glut1−/−* osteoblasts and that Smurf1 phosphorylation at S148 was higher in *Glut1−/−* than in control, *Glut1−/−;Ampka1+/−* and *Glut1−/−;Ampka1−/−* osteoblasts (Figure 5G-H). These results indicate that AMPK favors Runx2 proteasomal degradation by phosphorylating Smurf1.

This unanticipated regulation of Runx2 ubiquitination by AMPK allowed assessing selectively the ability of Runx2 to induce osteoblast differentiation when glucose uptake is compromised. This was achieved by generating $Glut1_{osx}$*−/−* embryos and $Glut1_{ocn}$*−/−* mice lacking one allele of *Smurf1*. This manipulation normalized Runx2 accumulation but did not restore mTORC1 signaling since p70S6K phosphorylation and Type I collagen synthesis remained low in $Glut1_{osx}$*−/−;Smurf1+/−* osteoblasts (Figure 5I-J). As a result and despite a normal accumulation of Runx2, skeletal development was equally delayed in $Glut1_{osx}$*−/−;Smurf1+/−* and $Glut1_{osx}$*−/−* embryos at E15.5 and E18.5 (Figure 5K-L). The cartilaginous area and the zone of *α1(X)Col*-expressing cells were as enlarged in $Glut1_{osx}$*−/−;Smurf1+/−* as in $Glut1_{osx}$*−/−* embryos (Figure 5M-N). Hence, Runx2 cannot induce proper osteoblast differentiation during embryogenesis if glucose uptake is hampered because protein synthesis is decreased (Figure 5O). Likewise, $Glut1_{ocn}$*−/−;Smurf1+/−* mice were as osteopenic as $Glut1_{ocn}$*−/−* mice (Figure S5C).

Glucose can initiate bone formation in *Runx2*-deficient embryos

We next asked if conversely, raising the extracellular concentration of glucose was sufficient to initiate Type I collagen synthesis in *Runx2*-deficient osteoblasts. To that end *Runx2fl/fl* osteoblasts (Takarada et al., 2013a) were infected with a *Cre*-expressing adenovirus (Figure S6A), these *Runx2−/−* osteoblasts were then cultured in a differentiation medium containing either 5 or 10mM glucose.

In *Runx2−/−* osteoblasts cultured in the presence of 5mM glucose, Glut1 accumulation and glucose consumption rate were decreased, phosphorylation of AMPKα1 was high, phosphorylation of p70S6K was low indicating that mTORC1 signaling was inhibited. As a result, ^{3}H-proline incorporation into collagen molecules and accumulation of Type I collagen were lower in *Runx2−/−* than in control osteoblasts (Figure 6A-C). In contrast, when the glucose concentration in the culture medium of *Runx2−/−* cells reached 10mM, the glucose consumption rate doubled, phosphorylation of AMPKα1 and p70S6K, incorporation rate of ^{3}H-proline into collagen molecules and the accumulation of Type I collagen were normalized in *Runx2−/−* cells, even though *Type I Collagen* gene expression was not changed (Figure 6A-D).

In view of these results we asked whether a chronic hyperglycemia would improve bone formation in *Runx2+/−* embryos. This was achieved by injecting streptozotocin (STZ, 150mg/kg) in *Runx2+/−* female mice as soon as a vaginal plug was seen. By decreasing the number of β-cells and circulating insulin levels this manipulation caused a severe hyperglycemia in E18.5 embryos (Figure 6E). We focused our analysis on bones forming through intramembranous ossification because they are the ones in which osteoblast

differentiation is hampered by *Runx2* haplo-insufficiency. While no difference was seen in WT embryos carried by STZ-treated mothers (Figure S6B), alcian blue/alizarin red staining of skeletal preparations showed that clavicles of E18.5 *Runx2*+/− embryos carried by STZ-treated mothers were twice as long as those of *Runx2*+/− embryos carried by vehicle-treated mothers (1.78±0.08 & 0.85±0.05 mm). Interparietal bones were also two-fold larger in *Runx2*+/− embryos carried by STZ-treated mothers (2.09±0.12 & 1.01±0.13 mm^2) than in those carried by control mothers and fontanelles of these embryos were less open than those of *Runx2*+/− embryos carried by vehicle-treated mothers (Figure 6F-G). Histological analyses showed the presence of mineralized bone trabeculae in the clavicles of E18.5 *Runx2*+/− embryos carried by STZ-treated mothers (Figure 6H-I). An immunohistochemistry analysis showed the presence of Type I collagen molecules in the clavicles of *Runx2*+/− embryos carried by STZ-treated mothers whereas only Type X collagen molecules were present in those of *Runx2*+/− embryos carried by vehicle-treated mothers (Figure 6J). Accumulation of Type I collagen was also increased in long bones of *Runx2*+/− embryos carried by STZ-treated mothers (Figure 6K-L). To further link the rescue of the bone phenotype in *Runx2*-deficient embryos to the increase in blood glucose levels, we repeated this experiment using lower doses of STZ (50 or 100mg/kg). One hundred mg/kg of STZ was toxic for β-cells since it decreased circulating insulin levels nearly two-fold without raising blood glucose levels in mothers or embryos (Figure 6E). This STZ dose did not correct the delay in bone development of *Runx2*-deficient embryos (Figure 6F-G). Thus, raising blood glucose levels normalized collagen synthesis and enhanced bone formation in *Runx2*+/− osteoblasts and embryos.

Although Type I collagen accumulation was also normalized in skeletal elements obtained form *Runx2*−/− embryos carried by STZ-treated mothers (Figure 6M), alcian blue/alizarin red staining of skeletal preparations failed to show any ECM mineralization in the skeleton of E18.5 *Runx2*−/− embryos carried by STZ-treated mothers (Figure S6C). This is probably explained by the fact that Runx2 regulates the expression of *Alkaline Phosphatase* (*Akp2*), a gene necessary for bone mineralization (Murshed et al., 2005) (Figure 6N, D).

A crosstalk between *Runx2* and *Glut1* coordinates osteoblast differentiation and bone formation

The results presented above delineated the influence of glucose uptake on osteoblast differentiation and bone formation but did not explain how these two events are coordinated in vivo. In addressing this question we interpreted the fact that *Glut1* expression and glucose uptake were decreased in *Runx2*+/− bones (Figure 7A-B) as suggesting that Runx2 regulates *Glut1* expression. *Runx1* expression in *Glut1/α1(I) Collagen*-expressing cells of the limb buds prompted us to test if Runx1 could trans-activate the *Glut1* promoter.

The *Glut1* promoter of the mouse and other vertebrate species has a canonical Runx binding site at −811bp (Figure 7C). Chromatin immunoprecipitation assays verified that Runx2 binds to this site (Figure 7D) and DNA co-transfection experiments performed in COS cells showed that *Runx2* or *Runx1* expression vectors could increase the activity of a *Glut1* promoter-luciferase reporter construct (p*Glut1-Luc*) only if this site was intact (Figure 7E). In agreement with these results, expression of *Glut1* was decreased in *Runx2*−/− and

increased in *Schnurri-3−/−* osteoblasts (*Shn3−/−*) that display an increase in Runx2 activity (Jones et al., 2006) (Figure 7F, S7A). These results explained why glucose uptake and mTORC1 activity were decreased in *Runx2−/−* and increased in *Shn3−/−* osteoblasts (Figure 7G, 6B).

If the feed-forward regulation between Glut1-dependent glucose uptake and Runx2 provides an explanation for the coordination of osteoblast differentiation and bone formation, $Glut1_{osx}$*+/−;Runx2+/−* embryos should display a delay in osteoblast differentiation similar to that of *Runx2−/−* embryos. Alcian blue/alizarin red staining of skeletal preparations showed that $Glut1_{osx}$*+/−;Runx2+/−* embryos were indistinguishable from *Runx2−/−* embryos up until E16.5 (Figure 7H, S7B). At E18.5, clavicles were barely detectable and most of the bones forming the skull were absent or severely hypoplastic in $Glut1_{osx}$*+/−;Runx2+/−* embryos (Figure 7I). Alcian blue staining of histological sections of long bones showed an enlargement of the area of hypertrophic chondrocytes and a cartilaginous ECM in E18.5 $Glut1_{osx}$*+/−;Runx2+/−* embryos (Figure 7J). *Osteocalcin* expression was undetectable in E18.5 $Glut1_{osx}$*+/−;Runx2+/−* skeletal elements, while it was present in single heterozygous embryos. Conversely, the area covered by *α1(X)Collagen*-expressing cells was greatly enlarged in E18.5 $Glut1_{osx}$*+/−;Runx2+/−* embryos (Figure 7K). The extent of the delay in osteoblast differentiation in $Glut1_{osx}$*+/−;Runx2+/−* embryos and mice explained why they all died peri-natally. This cross-regulation between *Runx2* and *Glut1* also determined the extent of bone formation since 3-month-old $Glut1_{ocn}$*+/−;Runx2+/−* mice had a low bone mass not seen either in $Glut1_{ocn}$*+/−* or *Runx2+/−* mice (Figure 7L).

Accounting for this severe phenotype and in agreement with the feed forward loop between glucose uptake in osteoblasts and Runx2, the accumulation of Glut1, Type I collagen and Runx2 was decreased more than 80% and phosphorylation of AMPK and Smurf1 was increased in $Glut1_{osx}$*+/−;Runx2+/−* compared to single heterozygous bones (Figure 7M). Hence, the cross-regulation of Runx2 and Glut1 is an amplification mechanism that determines the onset of osteoblast differentiation and the extent of bone formation throughout life. We also treated *Runx2+/−* mothers as soon as a vaginal plug was observed with STZ (150mg/kg). This dose of STZ raised blood glucose levels in mothers and embryos (Figure S7C), and increased bone formation in skeletal elements of the skull and in clavicles in $Glut1_{osx}$*+/−;Runx2+/−* embryos (Figure 7N).

Discussion

This study identifies glucose uptake in prospective osteoblasts as the earliest determinant of osteoblast differentiation and bone formation. It also shows that the coordination of osteoblast differentiation and bone formation throughout life is maintained by a feed-forward regulation between glucose uptake in osteoblasts and Runx2 accumulation. In addition, glucose uptake in osteoblasts is necessary for whole-body glucose homeostasis.

The bases of the coordination between osteoblast differentiation and bone formation

A striking feature of bone biology that has never been explained is that the synthesis of the main constituent of the bone ECM, Type I collagen, precedes the expression of and is not regulated by Runx2, the earliest transcriptional determinant of osteoblast differentiation.

This apparent disconnect between osteoblast differentiation and Type I collagen synthesis in the bone could be explained by a single mechanism controlling both aspects of osteoblast biology and acting upstream of Runx2. Our results suggest that this is the case and that this mechanism is glucose uptake in osteoblast progenitor cells. Glucose is the main nutrient of osteoblasts and is taken up by these cells in an insulin-independent manner through *Glut1* whose expression precedes the one of *Runx2*. Glucose uptake in osteoblasts favors osteoblast differentiation and bone formation through two distinct mechanisms. First, by inhibiting the activity of AMPK, glucose uptake enhances the activity of the mTORC1 pathway and therefore protein synthesis. Second and unexpectedly, glucose uptake inhibits another function of AMPK documented here, its ability to favor Runx2 ubiquitination in part via Smurf1. The two distinct functions of AMPK in osteoblasts revealed here explain why agonists of AMPK activity exert a deleterious influence on bone formation in vivo.

The *Glut1-Runx2* pathway described here could have clinical relevance. For instance, $Glut1_{osx}-/-$ embryos develop a CCD, a disease most often caused by a decrease in Runx2 expression. However, a significant number of CCD patients do not have any detectable mutations in *Runx2* (Puppin et al., 2005; Tessa et al., 2003). Conceivably in some of these patients, CCD may be caused by a decrease in glucose uptake or utilization in osteoblasts. If this was the case this would further support the notion that skeletal dysplasia may have a nutritional basis (Elefteriou et al., 2006). Moreover, the predilection of osteoblasts for glucose demonstrated here provides a plausible explanation for why children fed chronically a ketogenic diet experience poor longitudinal growth (Groesbeck et al., 2006).

The respective functions of glucose uptake and Runx2 in osteoblasts

Remarkably, restoring Runx2 accumulation in *Glut1−/−* cells did not translate into efficient bone formation in vivo simply because in osteoblasts unable to properly take up glucose, protein synthesis remains low regardless of the level of expression of *Runx2*. On the other hand, raising the extracellular concentration of glucose was sufficient to initiate bone formation even though osteoblasts were not fully differentiated in *Runx2+/−* embryos. Raising blood glucose levels in *Runx2−/−* embryos also increased collagen synthesis but that did not translate into the presence of a mineralized bone ECM because expression of *Akp2*, a gene necessary for bone ECM mineralization, is low in the absence of *Runx2*. Thus Runx2 is necessary for osteoblast differentiation and for bone ECM mineralization but, paradoxically, not for the synthesis of the main constituent of this ECM. In broader terms, the importance of glucose uptake in osteoblast differentiation described here raises the hypothesis that glucose uptake may be a more general determinant of cell differentiation during embryonic development. This may be particularly relevant for tissue like muscle that uptakes large amount of glucose.

Independently of its regulation of bone formation, glucose uptake in osteoblasts is necessary for another cardinal function of bone: the regulation of whole-body glucose metabolism. Indeed, through its regulation of Runx2 accumulation, glucose favors expression of the hormone osteocalcin.

The synergistic functions of glucose uptake and Runx2 in osteoblasts

How are osteoblast differentiation and bone formation coordinated throughout life? The fact that *Runx2−/−* and *Glut1−/−* osteoblasts had a similar metabolic profile suggested that this coordination might be explained if *Glut1* was a target gene of Runx2.

In support of this hypothesis, both molecular and genetic evidences identify Runx2 as a major regulator of *Glut1* expression and glucose uptake in osteoblasts. As a result, *Runx2−/−* osteoblasts bear metabolic similarities with *Glut1−/−* osteoblasts, $Glut1_{osx}$*+/−;Runx2+/−* embryos are similar to *Runx2−/−* embryos and $Glut1_{ocn}$*+/−;Runx2+/−* mice display an osteopenia not seen in either *Runx2+/−* or $Glut1_{ocn}$*+/−* mice. Hence, the reciprocal regulation between Glut1-mediated glucose uptake and Runx2 acts as an amplification chamber that determines the onset of osteoblast differentiation and the extent of bone formation throughout life. In addition, *Runx1* expression in the developing skeleton suggests that this Runx protein may regulate *Glut1* expression and thereby favors Type I collagen accumulation in prospective osteoblasts before E12.5.

In broader terms, results of this study cannot be separated from the recently described role of osteoblasts in maintaining glucose homeostasis in physiological and pathological situations (Lee et al., 2007; Ferron et al., 2010; Wei et al., 2014). The absolute necessity of glucose uptake for osteoblast differentiation, bone formation and glucose homeostasis documented here illustrates from the perspective of the osteoblast, the fundamental importance of the crosstalk between bone and glucose metabolism.

Experimental Procedures

Mice generation

To generate *Glut1fl/+* mice, a targeting vector harboring 2 LoxP sites flanking exon 3-10 of *Glut1* was electroporated into ES cells (CSL3,129/SvEvTac) (Figure S2A). Targeted ES cells were detected by southern blots and injected in 129Sv/EV blastocysts to generate chimeric mice. Chimeric mice were crossed with Gt(ROSA)26Sor$^{tm1(FLP1)Dym}$ mice to remove the *Neomycin* resistance cassette and to generate *Glut1fl/+* mice. *Glut1fl/+* mice were then crossed with *Dermo1-Cre(Yu et al., 2003), Osterix-Cre* (Rodda and McMahon, 2006) *or Ocn-Cre* mice (Zhang et al., 2002) to generate $Glut1_{osb}$*+/−* mice, whose progenies were intercrossed to obtain $Glut1_{dermo1}$*−/−*, $Glut1_{osx}$*−/−* and $Glut1_{ocn}$*−/−* mice, respectively. To generate *α1(I)Col-Glut1* transgenic mice, a cDNA fragment of the mouse *Glut1* was cloned into a plasmid containing a 2.3-kb *α1(I)* collagen promoter and microinjected using standard protocol. *Ampka1fl/fl* mice were obtained from The Jackson Laboratory(Nakada et al., 2010). *Runx2fl/fl* mice were generated as previously described (Takarada et al., 2013b; Hinoi et al., 2006). *Shn3+/−* and *Smurf1+/−* mice were generous gifts of Dr. L. Glimcher (Weill Cornell Medical College) and Dr. J. Wrana (U of Toronto, Canada) respectively (Jones et al., 2006; Narimatsu et al., 2009). Except for *α1(I)Col-Glut1* mice, which had been backcrossed to C57 background 5 times, all other mice analyzed were maintained on a C57/129 mixed background. Control littermates were analyzed in all experiments.

Cell culture

Mouse calvaria osteoblasts were isolated and cultured as described previously (Ducy and Karsenty, 1995). Osteoclast precursors (monocytes) were isolated by culturing bone marrow cells with αMEM/10% FBS containing M-CSF (10 ng/mL) for 6 days and then treated with RANKL (30 ng/mL) and M-CSF (10 ng/mL) for 7 days. C2C12 myoblasts (ATCC), mHippoE-14 embryonic mouse hippocampal hypothalamic cell Line (Cellutions biosystems) and COS-7 cells were cultured in DMEM/10% FBS. Glut1−/−, Raptor−/−, Runx2−/−, Glut1−/−;Ampka1+/−, Glut1−/−;Ampka1−/−, Ampka1+/− and *Ampka1*−/− calvaria osteoblasts were generated by infecting Glut1fl/fl, Raptorfl/fl, Runx2fl/fl, Glut1fl/fl;Ampka1fl/+, Glut1fl/fl;Ampka1fl/fl, Ampka1fl/+ or Ampka1fl/fl osteoblasts with either empty vector or *Cre*-expressing adenovirus (1:800 MOI) (University of Iowa). SiRNAs against *Tsc1* and *Tsc2* (Dharmacon) were transfected to primary osteoblasts according to manufacture's protocol.

Molecular biology and biochemistry

For quantifying gene expression, RNA samples were extracted using TRIZOL reagent (Invitrogen). One to 2 μg of total RNA was converted into cDNA using MMLV reverse transcriptase (Invitrogen). QPCR analyses were performed using CFX-Connect realtime PCR system (Bio-Rad). Relative expression levels of each gene were normalized to the levels of 18S ribosomal RNA or *β-actin*. Western blot analyses were carried out using standard protocol. All antibodies were obtained from Cell Signaling Technology, except the anti-GLUT1 (EMD Millipore), anti-COL1A1, anti-RUNX2, anti-SMURF1 (Santa Cruz), anti-Phospho-Ser148 Smurf1 (Genescript) and anti-β-ACTIN (Sigma). Quantification of Western blots was performed using Image J. Protein levels were quantified and normalized to ACTIN or GADPH levels. Relative protein levels were calculated with respect to control samples. All western blot experiments were repeated at least three times, with different samples.

Glucose consumption and uptake assay

For glucose consumption measurements, following 16-hr incubation with osteoblasts, glucose concentration in the culture medium was assayed with Glucose Assay Kit (Biovision). Glucose uptake was determined by the uptake rate of 2-[U-^{14}C] deoxyglucose (2-DG) in cells. Following 1hr fast in glucose free KRH buffer (50mM HEPES pH7.4, 136mM NaCl, 4.7mM KCl, 1.25mM MgSO4, 1.25mM CaCl2 and 0.1% BSA), cells were cultured in KRH buffer containing 100chkM 2-deoxyglucose and 0.5chkCi/ml 2-^{14}C-DG (287mCi/mmol, Perkin Elmer, NEC495A) for 1hr. For glucose uptake in bones, 10μCi of 2-^{14}C-DG were IP injected in mice at random feed state for 1h calvariae were then collected for analysis. The amount of 2-^{14}C-DG in total cell or bone lyses was quantified by liquid scintillation counter (WALLAC 1409) and normalized to protein content (Bio-Rad).

Skeleton preparation, Bone histology and in situ hybridization

Skeleton preparations and Alcian blue/alizarin red staining were carried out according to standard protocols (McLeod, M.J. 1980). Bone histology analyses including Von Kossa staining and alcian blue staining were performed with histological sections of femurs or

clavicle bones using standard protocols. For all skeletal analyses, at least 3 litters for each embryonic stage and at least 5 embryos for each genotype were examined. Bone histomorphometry analyses were performed on L3 and L4 vertebrae as described previously (Chappard et al., 1987; Parfitt et al., 1987). Von Kossa/van Gieson Staining, toluidine blue staining and calcein double-labeling were performed to measure mineralized bone volume over the total tissue volume (BV/TV), osteoblast number per tissue area, (N.Ob/T.Ar), mineralization apposition rate (MAR) and bone formation rate per bone surface (BFR/BS). For in situ hybridization, tissues were fixed in 4% paraformaldehyde/PBS overnight at 4°C and then afte r serial of dehydrations embedded in paraffin and sectioned at 5μm. In situ hybridization was performed using ^{35}S-labeled riboprobe as described (Ducy et al., 1997). The Runx1, Runx3, Runx2, α1(I)Col, α1(II)Col, α 1(X)Col, Osteocalcin and *Bsp* probes have been previously described (Takeda et al., 2001). The *Glut1* probe is a 500-bp fragment of the *Glut1* 3′ untranslated region (see Extended Method and Material for sequence information). Hybridizations were performed overnight at 55°C, and washes were performed at 63°C.

Statistics

All data are presented as mean ± standard error of mean. Statistical analyses were performed using unpaired, two-tailed Student's *t* test for comparison between two groups, ANOVA test for experiments involving more than two groups. For all experiments, * denotes $P \leq 0.05$, # denotes $P \leq 0.001$ compared to control.

Supplementary Material

Refer to Web version on PubMed Central for supplementary material.

Acknowledgements

We thank Drs. P. Ducy, J. Wrana, J. Shim and L. Glimcher for critical reading of the manuscript and reagents. This work was supported by NIH grant R01AR045548 (G.K.), Columbia University Mandl Connective Tissue Research Fellowship (J. W.) and Honjo International Scholarship (J. S.).

Reference

Long F. Building strong bones: molecular regulation of the osteoblast lineage. Nat Rev Mol Cell Biol. 2012; 13:27–38. [PubMed: 22189423]

Karsenty G, Kronenberg HM, Settembre C. Genetic control of bone formation. Annu Rev Cell Dev Biol. 2009; 25:629–648. [PubMed: 19575648]

Vuorio E, de Crombrugghe B. The family of collagen genes. Annu Rev Biochem. 1990; 59:837–872. [PubMed: 2197991]

Kern B, Shen J, Starbuck M, Karsenty G. Cbfa1 contributes to the osteoblast-specific expression of type I collagen genes. J Biol Chem. 2001; 276:7101–7107. [PubMed: 11106645]

Lee NK, Sowa H, Hinoi E, Ferron M, et al. Endocrine regulation of energy metabolism by the skeleton. Cell. 2007; 130:456–469. [PubMed: 17693256]

Ferrannini E, Simonson DC, Katz LD, Reichard G Jr. et al. The disposal of an oral glucose load in patients with non-insulin-dependent diabetes. Metabolism. 1988; 37:79–85. [PubMed: 3275860]

Yu K, Xu J, Liu Z, Sosic D, et al. Conditional inactivation of FGF receptor 2 reveals an essential role for FGF signaling in the regulation of osteoblast function and bone growth. Development. 2003; 130:3063–3074. [PubMed: 12756187]

Rodda SJ, McMahon AP. Distinct roles for Hedgehog and canonical Wnt signaling in specification, differentiation and maintenance of osteoblast progenitors. Development. 2006; 133:3231–3244. [PubMed: 16854976]

Mundlos S, Otto F, Mundlos C, Mulliken JB, et al. Mutations involving the transcription factor CBFA1 cause cleidocranial dysplasia. Cell. 1997; 89:773–779. [PubMed: 9182765]

Lee B, Thirunavukkarasu K, Zhou L, Pastore L, et al. Missense mutations abolishing DNA binding of the osteoblast-specific transcription factor OSF2/CBFA1 in cleidocranial dysplasia. Nat Genet. 1997; 16:307–310. [PubMed: 9207800]

Yamashita H, Takenoshita M, Sakurai M, Bruick RK, et al. A glucose-responsive transcription factor that regulates carbohydrate metabolism in the liver. Proc Natl Acad Sci U S A. 2001; 98:9116–9121. [PubMed: 11470916]

Zhang M, Xuan S, Bouxsein ML, von Stechow D, et al. Osteoblast-specific knockout of the insulin-like growth factor (IGF) receptor gene reveals an essential role of IGF signaling in bone matrix mineralization. J Biol Chem. 2002; 277:44005–44012. [PubMed: 12215457]

Jeyapalan AS, Orellana RA, Suryawan A, O'Connor PM, et al. Glucose stimulates protein synthesis in skeletal muscle of neonatal pigs through an AMPK- and mTOR-independent process. Am J Physiol Endocrinol Metab. 2007; 293:E595–603. [PubMed: 17551002]

Mayer FV, Heath R, Underwood E, Sanders MJ, et al. ADP regulates SNF1, the Saccharomyces cerevisiae homolog of AMP-activated protein kinase. Cell Metab. 2011; 14:707–714. [PubMed: 22019086]

Woods A, Munday MR, Scott J, Yang X, et al. Yeast SNF1 is functionally related to mammalian AMP-activated protein kinase and regulates acetyl-CoA carboxylase in vivo. J Biol Chem. 1994; 269:19509–19515. [PubMed: 7913470]

Wilson WA, Hawley SA, Hardie DG. Glucose repression/derepression in budding yeast: SNF1 protein kinase is activated by phosphorylation under derepressing conditions, and this correlates with a high AMP:ATP ratio. Curr Biol. 1996; 6:1426–1434. [PubMed: 8939604]

Bolster DR, Crozier SJ, Kimball SR, Jefferson LS. AMP-activated protein kinase suppresses protein synthesis in rat skeletal muscle through down-regulated mammalian target of rapamycin (mTOR) signaling. J Biol Chem. 2002; 277:23977–23980. [PubMed: 11997383]

Reiter AK, Bolster DR, Crozier SJ, Kimball SR, et al. Repression of protein synthesis and mTOR signaling in rat liver mediated by the AMPK activator aminoimidazole carboxamide ribonucleoside. Am J Physiol Endocrinol Metab. 2005; 288:E980–988. [PubMed: 15613684]

Zhao M, Qiao M, Oyajobi BO, Mundy GR, et al. E3 ubiquitin ligase Smurf1 mediates core-binding factor alpha1/Runx2 degradation and plays a specific role in osteoblast differentiation. J Biol Chem. 2003; 278:27939–27944. [PubMed: 12738770]

Takarada T, Hinoi E, Nakazato R, Ochi H, et al. An analysis of skeletal development in osteoblast-specific and chondrocyte-specific runt-related transcription factor-2 (Runx2) knockout mice. J Bone Miner Res. 2013a; 28:2064–2069. [PubMed: 23553905]

Murshed M, Harmey D, Millan JL, McKee MD, et al. Unique coexpression in osteoblasts of broadly expressed genes accounts for the spatial restriction of ECM mineralization to bone. Genes Dev. 2005; 19:1093–1104. [PubMed: 15833911]

Jones DC, Wein MN, Oukka M, Hofstaetter JG, et al. Regulation of adult bone mass by the zinc finger adapter protein Schnurri-3. Science. 2006; 312:1223–1227. [PubMed: 16728642]

Puppin C, Pellizzari L, Fabbro D, Fogolari F, et al. Functional analysis of a novel RUNX2 missense mutation found in a family with cleidocranial dysplasia. J Hum Genet. 2005; 50:679–683. [PubMed: 16244783]

Tessa A, Salvi S, Casali C, Garavelli L, et al. Six novel mutations of the RUNX2 gene in Italian patients with cleidocranial dysplasia. Hum Mutat. 2003; 22:104. [PubMed: 12815605]

Elefteriou F, Benson MD, Sowa H, Starbuck M, et al. ATF4 mediation of NF1 functions in osteoblast reveals a nutritional basis for congenital skeletal dysplasiae. Cell Metab. 2006; 4:441–451. [PubMed: 17141628]

Groesbeck DK, Bluml RM, Kossoff EH. Long-term use of the ketogenic diet in the treatment of epilepsy. Dev Med Child Neurol. 2006; 48:978–981. [PubMed: 17109786]

Ferron M, Wei J, Yoshizawa T, Del Fattore A, et al. Insulin signaling in osteoblasts integrates bone remodeling and energy metabolism. Cell. 2010; 142:296–308. [PubMed: 20655470]

Wei J, Hanna T, Suda N, Karsenty G, et al. Osteocalcin Promotes beta-Cell Proliferation During Development and Adulthood Through Gprc6a. Diabetes. 2014; 63:1021–1031. [PubMed: 24009262]

Nakada D, Saunders TL, Morrison SJ. Lkb1 regulates cell cycle and energy metabolism in haematopoietic stem cells. Nature. 2010; 468:653–658. [PubMed: 21124450]

Takarada T, Hinoi E, Nakazato R, Ochi H, et al. An analysis of skeletal development in osteoblast- and chondrocyte-specific Runx2 knockout mice. J Bone Miner Res. 2013b

Hinoi E, Bialek P, Chen YT, Rached MT, et al. Runx2 inhibits chondrocyte proliferation and hypertrophy through its expression in the perichondrium. Genes Dev. 2006; 20:2937–2942. [PubMed: 17050674]

Narimatsu M, Bose R, Pye M, Zhang L, et al. Regulation of planar cell polarity by Smurf ubiquitin ligases. Cell. 2009; 137:295–307. [PubMed: 19379695]

Ducy P, Karsenty G. Two distinct osteoblast-specific cis-acting elements control expression of a mouse osteocalcin gene. Mol Cell Biol. 1995; 15:1858–1869. [PubMed: 7891679]

Chappard D, Palle S, Alexandre C, Vico L, et al. Bone embedding in pure methyl methacrylate at low temperature preserves enzyme activities. Acta Histochem. 1987; 81:183–190. [PubMed: 3111154]

Parfitt AM, Drezner MK, Glorieux FH, Kanis JA, et al. Bone histomorphometry: standardization of nomenclature, symbols, and units. Report of the ASBMR Histomorphometry Nomenclature Committee. J Bone Miner Res. 1987; 2:595–610. [PubMed: 3455637]

Ducy P, Zhang R, Geoffroy V, Ridall AL, et al. Osf2/Cbfa1: a transcriptional activator of osteoblast differentiation. Cell. 1997; 89:747–754. [PubMed: 9182762]

Takeda S, Bonnamy JP, Owen MJ, Ducy P, et al. Continuous expression of Cbfa1 in nonhypertrophic chondrocytes uncovers its ability to induce hypertrophic chondrocyte differentiation and partially rescues Cbfa1-deficient mice. Genes Dev. 2001; 15:467–481. [PubMed: 11230154]

Highlights

- Osteoblasts are addicted to glucose.
- Glucose uptake is needed for osteoblast differentiation and bone formation.
- Runx2 is necessary Glut1 expression in prospective osteoblasts
- Glut1 and Runx2 crosstalk determines osteoblast differentiation and bone formation.

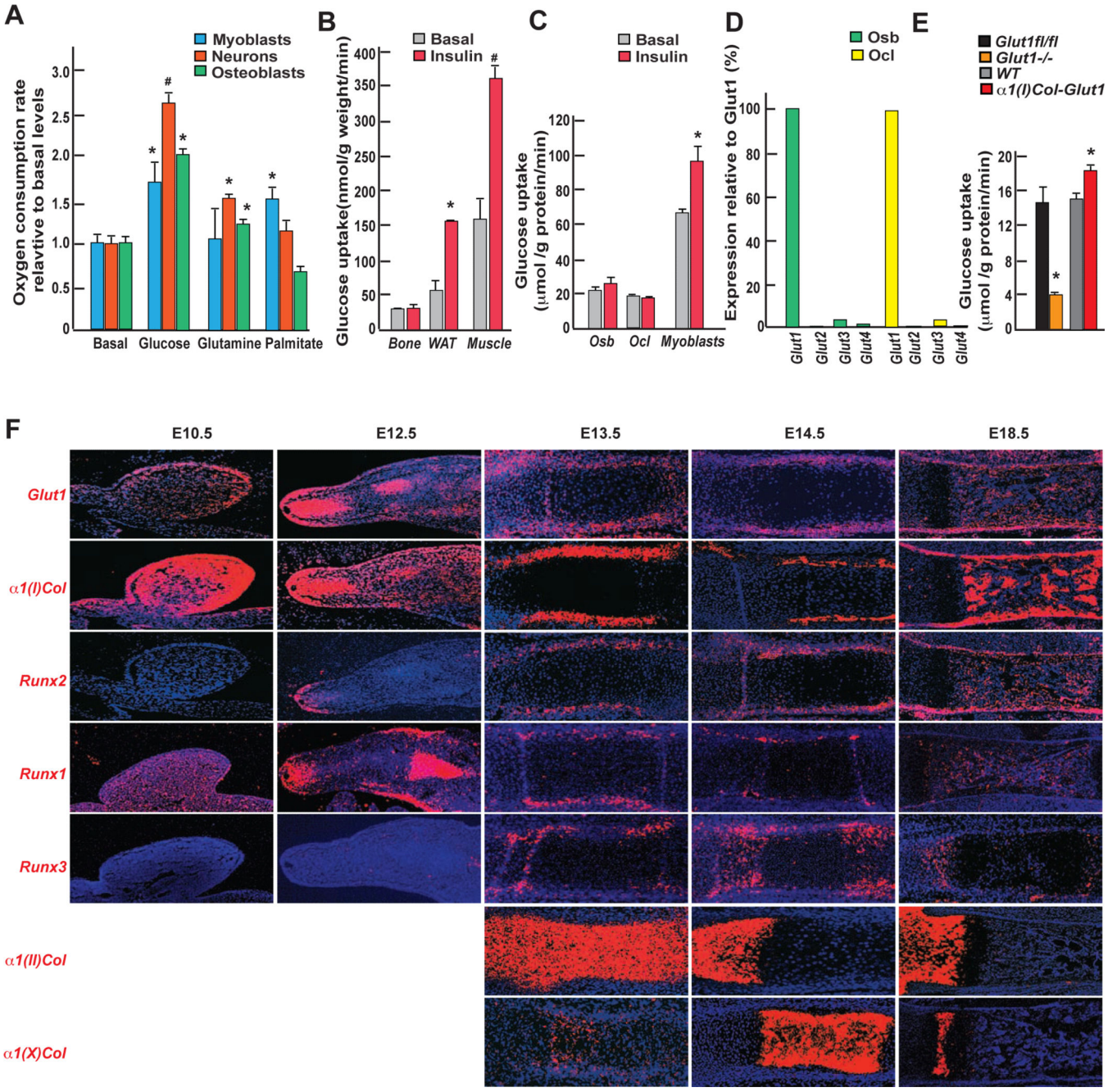

Figure 1. Insulin-independent glucose uptake in osteoblasts

A. Oxygen consumption rate (OCR) of osteoblasts, C2C12 myoblasts or hippocampal neurons incubated with vehicle, 10mM glucose, 2mM glutamine or 300μM palmitate in 1X KHB buffer for 2hrs (n=8).

B. Glucose uptake measured by euglycemic hyperinsulinemic clamps in femurs, white adipose tissue and gastrocnemius muscle of WT mice before or after insulin infusion (2.5 mU/kg/min) (n=4);

C. Uptake rate of 2-DG in osteoblasts (Osb), osteoclasts (Ocl) and myoblasts (n=3).

D. Expression of class I *Gluts* in osteoblasts and osteoclasts assayed by qPCR.

E. Uptake rate of 2-DG in *Glut1fl/fl*, *Glut1−/−*, WT and *α1(I)Col-Glut1* osteoblasts (n=6-8). **F**. In situ hybridization analysis of *Glut1* (a-e), *α1(I) Collagen* (f-j), *Runx2* (k-o) *Runx1*(p-t), *Runx3* (u-v), *α1(II) Collagen* (z-b1) and *α1(X) Collagen* (c1-e1) in hind-limbs during embryonic development.

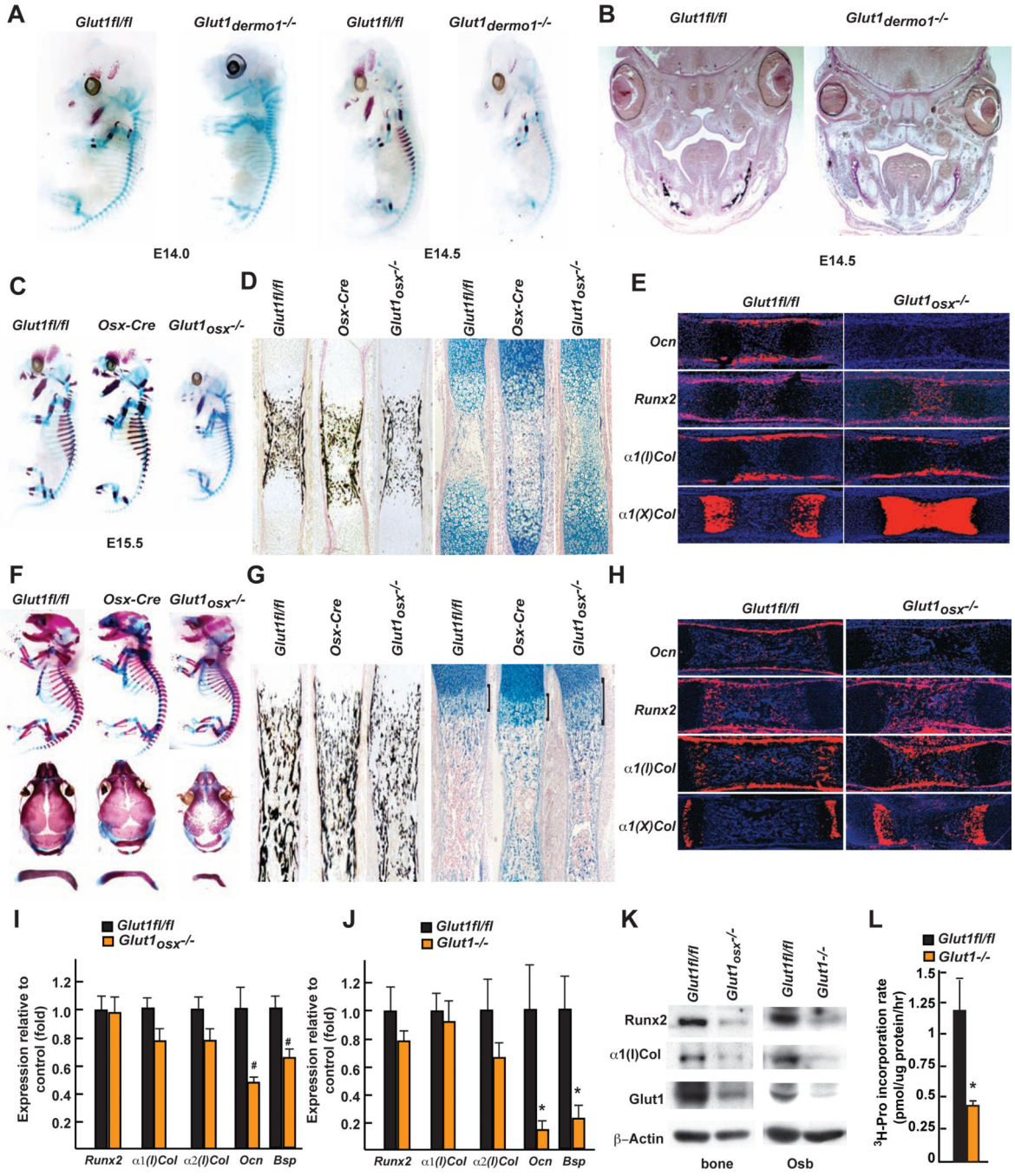

Figure 2. Glucose uptake is necessary for osteoblast differentiation during development

A. Alcian blue/alizarin red staining of skeletal preparations of E14.0 and 14.5 *Glut1*$_{dermo1}$*−/−* and *Glut1fl/fl* embryos.

B. Von Kossa staining of skull sections of E14.5 *Glut1*$_{dermo1}$*−/−* and *Glut1fl/fl* embryos.

C and **F**. Alcian blue/alizarin red staining of skeletal preparations of E15.5 (C) and 18.5 (F) *Glut1*$_{osx}$*−/−*, *Glut1fl/fl* and *Osx-cre* embryos.

D and **G.** Von Kossa or alcian blue staining of femur from E15.5 (D) and 18.5 (G) *Glut1*$_{osx}$*−/−*, *Glut1fl/fl* and *Osx-cre* embryos.

E and **H**. In situ hybridization analysis of *Osteocalcin, α1(I), α1(X) Collagen* and *Runx2* expression in E15.5 (E) and 18.5 (H) $Glut1_{osx}-/-$ and *Glut1fl/fl* femurs.

I. Expression of osteoblast markers in E18.5 $Glut1_{osx}-/-$ and *Glut1fl/fl* femurs (n=9).

J. Expression of osteoblast marker genes in *Glut1fl/fl* and *Glut1−/−* osteoblasts. (n=6)

K. α1(I) Collagen and Runx2 accumulations in E18.5 $Glut1_{osx}-/-$ and *Glut1fl/fl* femurs and *Glut1fl/fl* and *Glut1−/−* osteoblasts.

L. ^{3}H-proline incorporation in collagen in *Glut1fl/fl* and *Glut1−/−* osteoblasts (n=6).

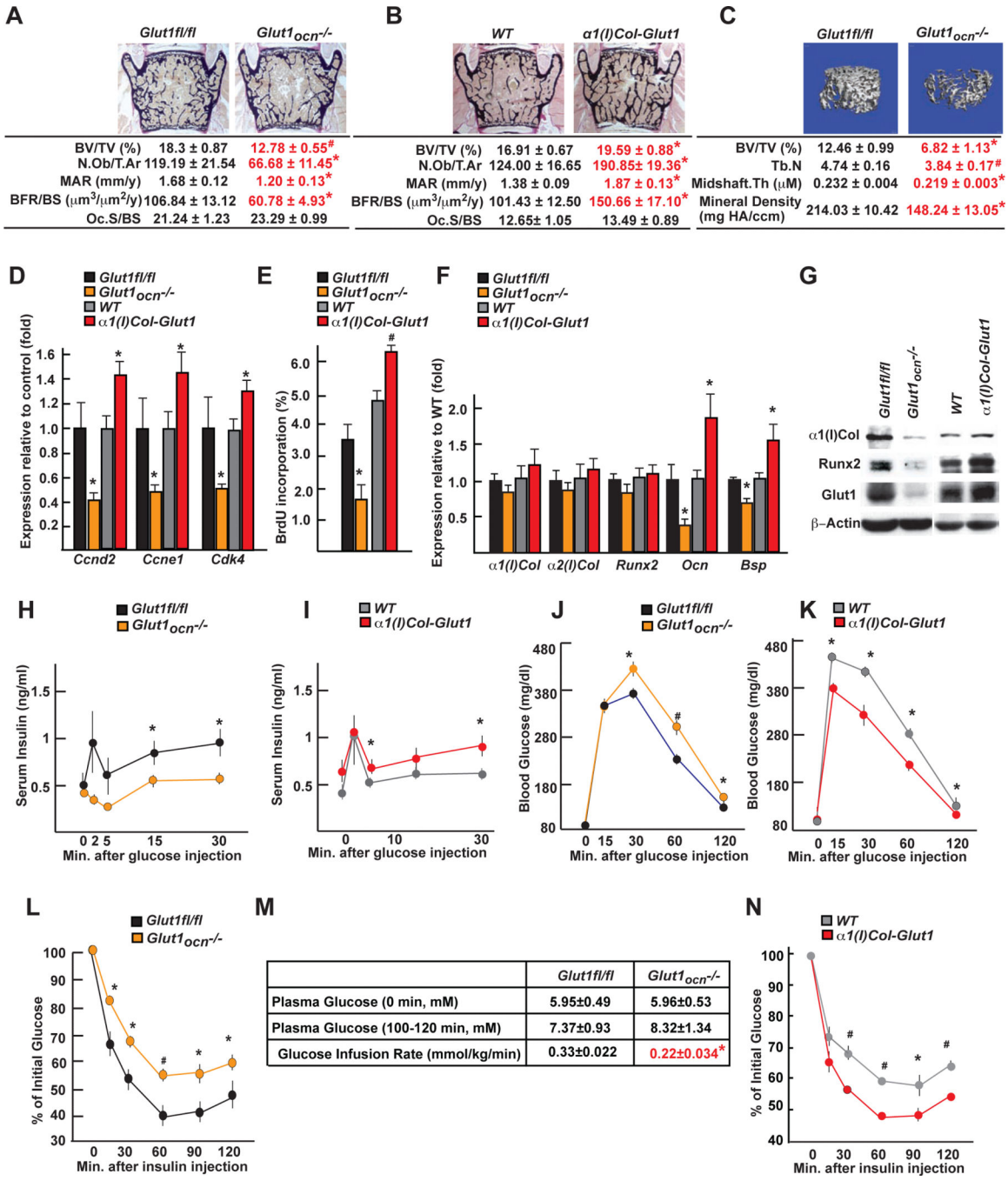

Figure 3. Glucose uptake in osteoblasts is necessary for bone formation and glucose homeostasis post-natally

A and **B**. Histomorphometric analysis of L4 vertebrae of 3 month-old *lut1fl/fl*, *Glut1*$_{ocn}$$^{-/-}$, WT and *α1(I)Col-Glut1* male mice (n=9-11).

C. μCT analysis of proximal femurs of *Glut1fl/fl* and *Glut1*$_{ocn}$$^{-/-}$ male mice (n=7).

D. Expression of *Ccnd2*, *Ccne1* and *Cdk4* in femurs of 3 month-old *Glut1fl/fl*, *Glut1*$_{ocn}$$^{-/-}$, WT and *α1(I)Col-Glut1* mice (n=6).

E. BrdU incorporation in calvaria of P14 *Glut1fl/fl*, *Glut1*$_{ocn}$−/−, WT and *α1(I)Col-Glut1* mice (n=5-8).

F. Expression of osteoblast marker genes in femurs of 3 month-old *Glut1fl/fl*, *Glut1*$_{ocn}$−/−, WT and *α1(I)Col-Glut1* mice (n=8).

G. α1(I) Collagen and Runx2 accumulations in femurs of 3 month-old *Glut1fl/fl*, *Glut1*$_{ocn}$−/−, WT and *α1(I)Col-Glut1* mice.

H-I. GSIS in 3 month-old *Glut1fl/fl*, *Glut1*$_{ocn}$−/−, WT and *α1(I)Col-Glut1* mice (n=10-11).

J-K. GTT in 3 month-old *Glut1fl/fl*, *Glut1*$_{ocn}$−/−, WT and *α1(I)Col-Glut1* mice (n=5-10).

L-N. ITT in 3 month-old *Glut1fl/fl*, *Glut1*$_{ocn}$−/−, WT and *α1(I)Col-Glut1* mice (n=8-10).

M. Glucose infusion rate in 3 month-old *Glut1fl/fl* and *Glut1*$_{ocn}$−/− mice (n=6).

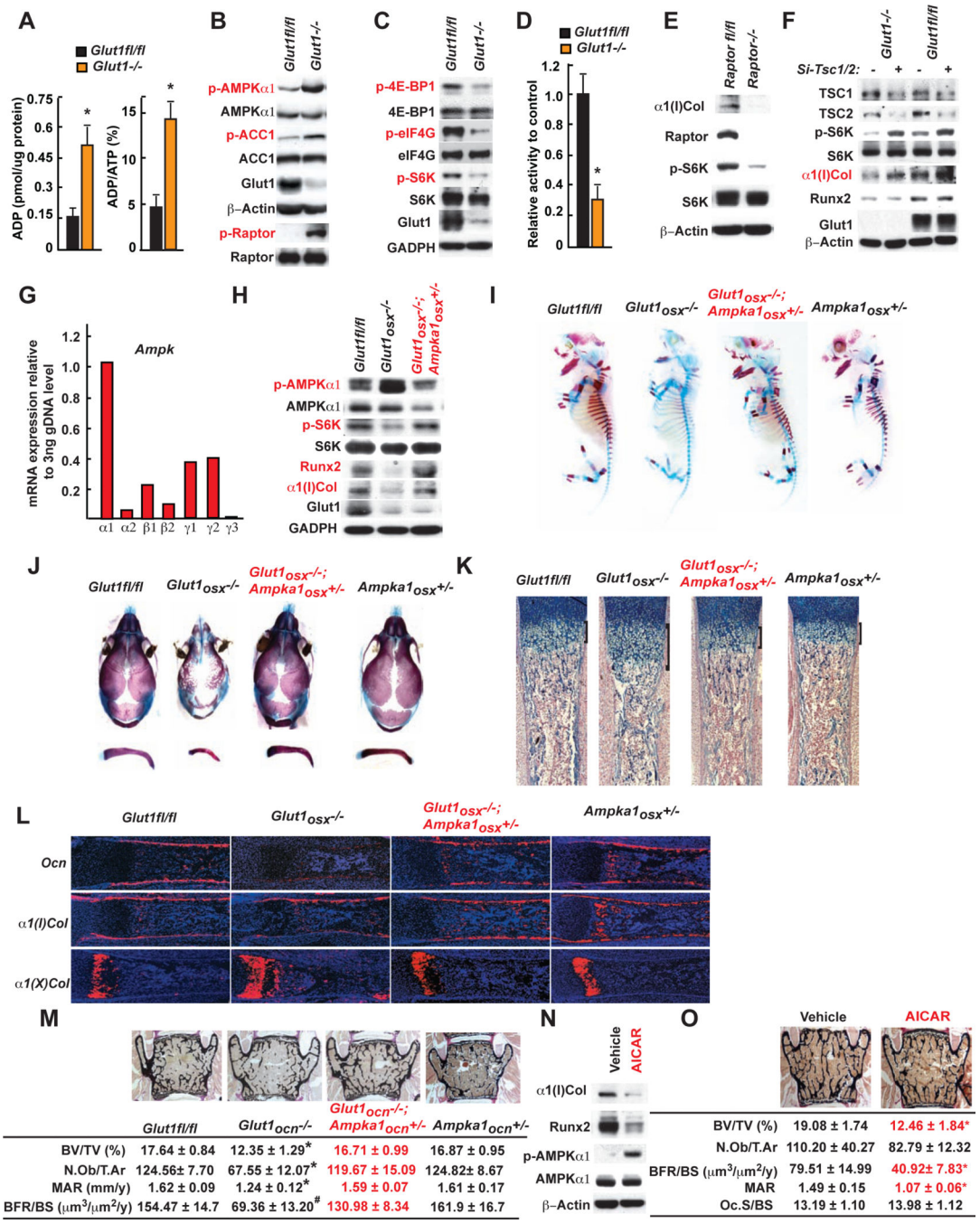

Figure 4. Glucose uptake favors osteoblast differentiation and bone formation by inhibiting AMPK

A. ADP content and ADP/ATP ratio in WT and *Glut1−/−* osteoblasts (n=6).

B-C. AMPK, ACC1, Raptor (B), p70S6K, 4E-BP1 and eIF4G phosphorylation in WT and *Glut1−/−* osteoblasts.

D. Kinase assay of immune-precipitated mTORC1 complex in WT and *Glut1−/−* osteoblasts (n=3).

E. Raptor, p70S6K phosphorylation and α1(I)Collagen accumulations in WT and *Raptor−/−* osteoblasts.

F. TSC1, TSC2, and p70S6K phosphorylation, α1(I)Collagen and Runx2 accumulations in WT and *Glut1−/−* osteoblasts transfected with SiRNAs targeting *Tsc1* and *Tsc2* or scrambled SiRNA.

G. Expression of various AMPK subunits in osteoblasts.

H. AMPK and p70S6K phosphorylation, Runx2 and α1(I)Collagen accumulations in *Glut1fl/fl*, $Glut1_{osx}$*−/−* and $Glut1_{osx}$*−/−;*$Ampka1_{osx}$*+/−* osteoblasts.

I-J. Alcian blue/alizarin red staining of skeletal preparations of E15.5 (I) and 18.5 (J) *Glut1fl/fl*, $Glut1_{osx}$*−/−*, $Ampka1_{osx}$*+/−* and $Glut1_{osx}$*−/−;*$Ampka1_{osx}$*+/−* embryos.

K. Alcian blue staining of histological sections of femurs of E18.5 *Glut1fl/fl*, $Glut1_{osx}$*−/−*, $Ampka1_{osx}$*+/−* and $Glut1_{osx}$*−/−;*$Ampka1_{osx}$*+/−* embryos.

L. In situ hybridization analysis of *Osteocalcin*, *α1(I)*, *α1(II)* and *α1(X) Collagen* expression in femurs of E18.5 *Glut1fl/fl*, $Glut1_{osx}$*−/−*, $Ampka1_{osx}$*+/−* and $Glut1_{osx}$*−/−;*$Ampka1_{osx}$*+/−* embryos.

M. Histomorphometric analysis of L4 vertebrae of 3 month-old of *Glut1fl/fl*, $Glut1_{ocn}$*−/−*, $Ampka1_{ocn}$*+/−* and $Glut1_{ocn}$*−/−;*$Ampka1_{ocn}$*+/−* male mice (n=7-10).

N. AMPK phosphorylation, Runx2 and α1(I)Collagen accumulations in osteoblasts treated with vehicle or AICAR (0.1mM) for 16 hrs.

O. Histomorphometric analysis of L4 vertebrae of 3 month-old of WT mice treated with vehicle or AICAR (250mg/kg/day) for 8 weeks (n=6).

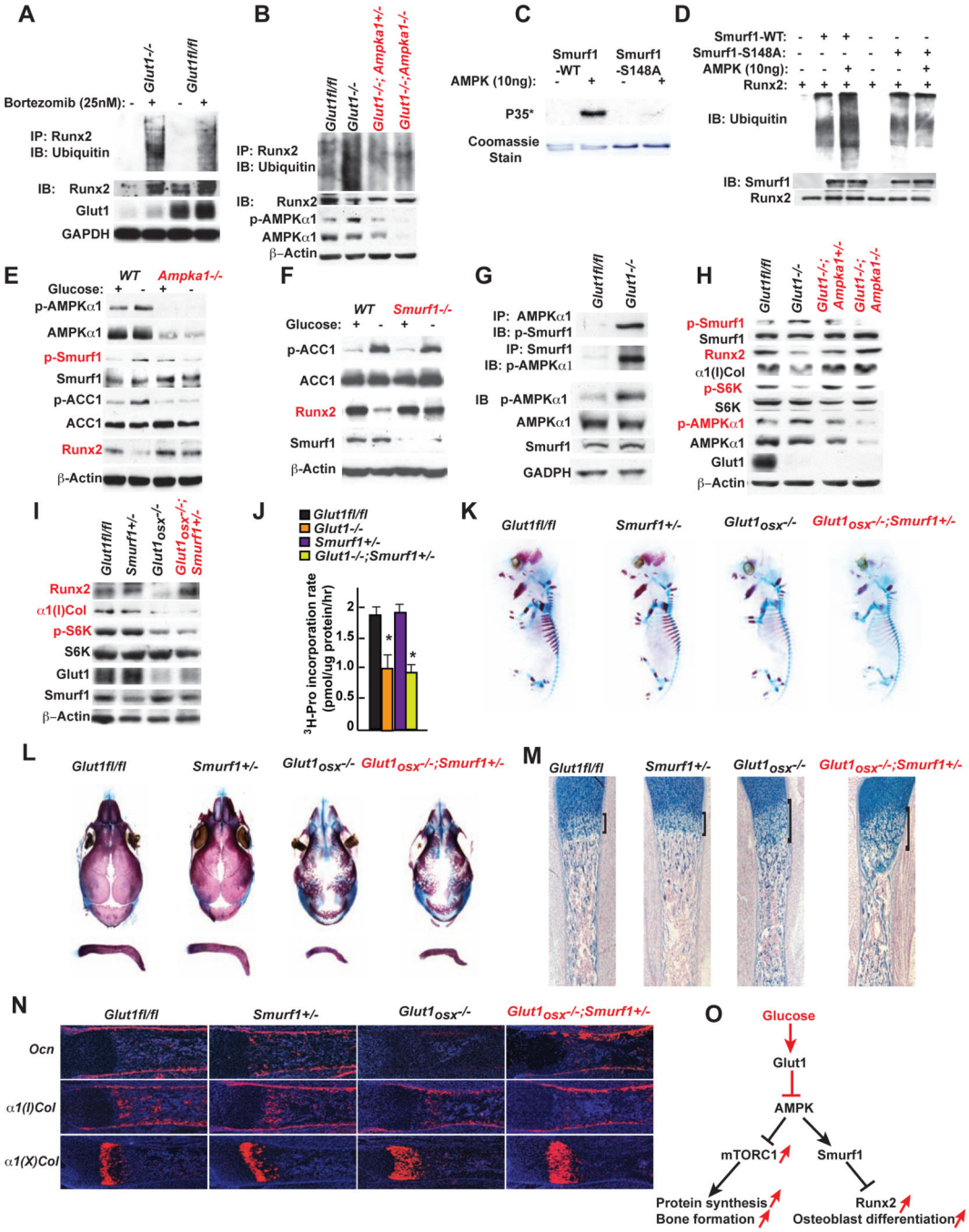

Figure 5. Runx2 cannot induce proper osteoblast differentiation if glucose uptake is hampered

A. Ubiquitination of immune-precipitated Runx2 in WT and *Glut1−/−* osteoblasts treated with 25nM Bortezomib for 16hrs.

B. Ubiquitination of immune-precipitated Runx2 in WT, *Glut1−/−*, *Glut1−/−Ampka1+/−* and *Glut1−/− Ampka1−/−* osteoblasts treated with 25nM Bortezomib for 16hrs.

C. In vitro AMPK phosphorylation assay of Smurf1 and Smurf1-S148/A.

D. In vitro ubiquitination assay of Smurf1 and Smurf1-S148/A phosphorylated by AMPK.

E-F. Runx2 and α1(I)Collagen accumulations, AMPK and Smurf1 phosphorylation in WT, *Smurf1*−/− (E) and *Ampka1*−/− (F) osteoblasts cultured with or without glucose for 16 hrs.
G. Co-immunoprecipitation of AMPKα1 and Smurf1 in WT and *Glut1*−/− osteoblasts.
H. Runx2 and α1(I)Collagen accumulations, AMPKα1, p70S6K and Smurf1 phosphorylation in WT, *Glut1*−/−, *Glut1*−/− *Ampka1*+/− and *Glut1*−/− *Ampka1*−/− osteoblasts.
I. Runx2 and α1(I)Collagen accumulations and p70S6K phosphorylation in *Glut1fl/fl*, $Glut1_{osx}$−/− and $Glut1_{osx}$−/−;*Smurf1*+/− osteoblasts.
J. ^{3}H-proline incorporation in collagen molecules in *Glut1fl/fl*, *Glut1*−/− and *Glut1*−/−;*Smurf1*+/− osteoblasts (n=6).
K-L. Alcian blue/alizarin red staining of skeletal preparations of E15.5 (G) and 18.5 (I) *Glut1fl/fl*, *Smurf1*+/−, $Glut1_{osx}$−/− and $Glut1_{osx}$−/−;*Smurf1*+/− embryos.
M. Alcian blue staining of sections of femurs of E18.5 *Glut1fl/fl*, $Glut1_{osx}$−/− and $Glut1_{osx}$−/−;*Smurf1*+/− embryos.
N. In situ hybridization analysis of *Osteocalcin*, *α1(I)* and *α1(X) Collagens* expression, in femurs of E18.5 *Glut1fl/fl*, $Glut1_{osx}$−/− and $Glut1_{osx}$−/−;*Smurf1*+/− embryos.
O. Schematic representation of the pathways triggered by glucose uptake in osteoblasts.

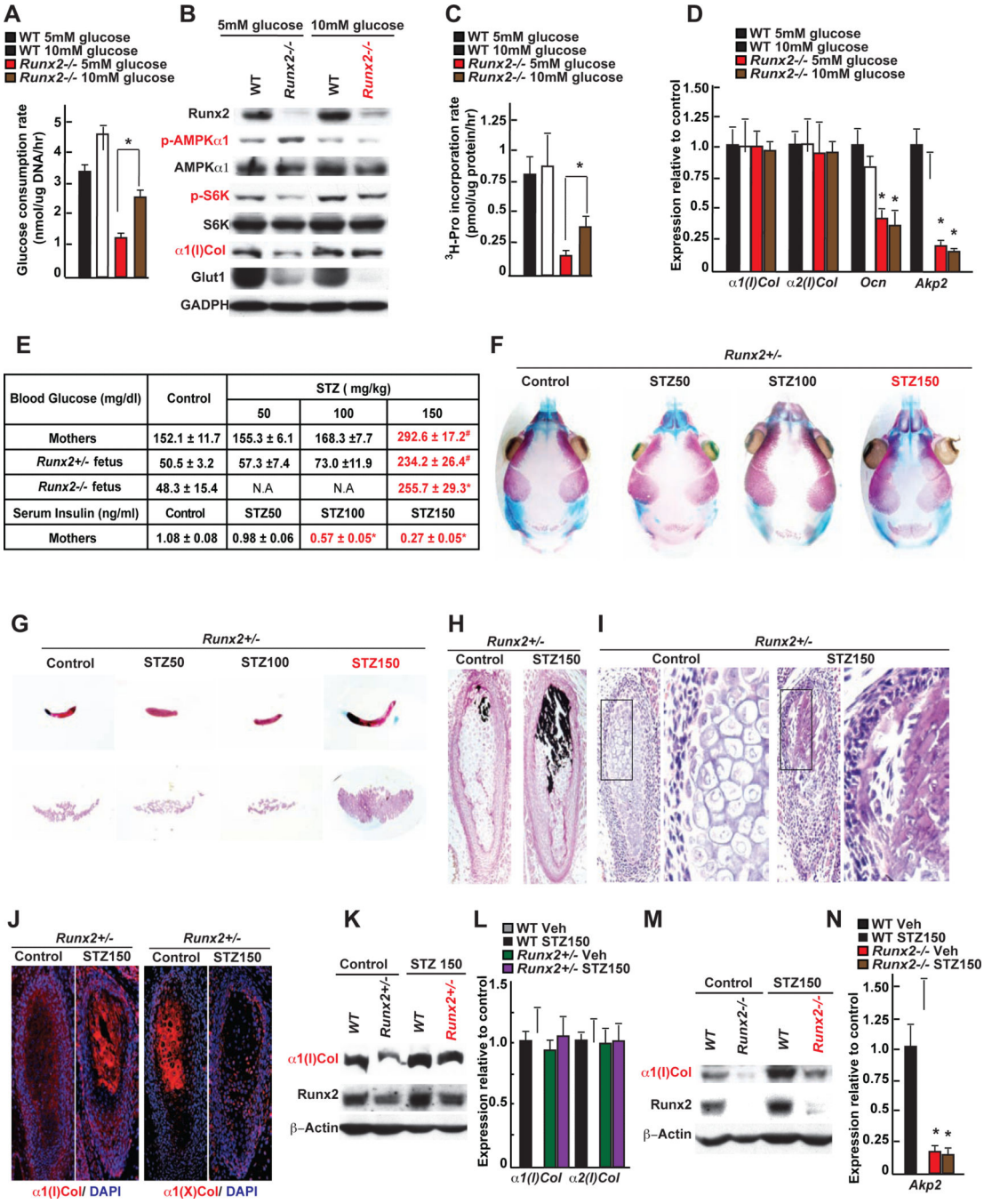

Blood Glucose (mg/dl)	Control	STZ (mg/kg)		
		50	100	150
Mothers	152.1 ± 11.7	155.3 ± 6.1	168.3 ±7.7	292.6 ± 17.2#
Runx2+/- fetus	50.5 ± 3.2	57.3 ±7.4	73.0 ±11.9	234.2 ± 26.4#
Runx2-/- fetus	48.3 ± 15.4	N.A	N.A	255.7 ± 29.3*
Serum Insulin (ng/ml)	Control	STZ50	STZ100	STZ150
Mothers	1.08 ± 0.08	0.98 ± 0.06	0.57 ± 0.05*	0.27 ± 0.05*

Figure 6. Glucose can initiate bone formation in Runx2-deficient embryos

A. Glucose consumption rate in WT and *Runx2−/−* osteoblasts cultured with 5 or 10mM glucose for 16hrs.

B. Runx2, α1(I)Collagen and Glut1 accumulations, AMPKα1 and p70S6K phosphorylation in WT and *Runx2−/−* osteoblasts cultured with 5 or 10mM glucose for 14 days.

C. ^{3}H-proline incorporation in collagen molecules in WT and *Runx2−/−* osteoblasts cultured with 5 or 10mM glucose for 14 days (n=5).

D. qPCR analysis of osteoblast marker genes in WT and *Runx2−/−* osteoblasts cultured with 5 or 10mM glucose for 14 days (n=6).

E. Blood glucose and insulin levels in STZ (50, 100, 150mg/kg) and vehicle-treated *Runx2+/-* mothers and progenies at E18.5 (n=5-12).

F-G. Alcian blue/alizarin red staining of the skull (F), clavicles and interparietal bones (G) of E18.5 *Runx2+/-* embryos carried by STZ (50, 100, or 150mg/kg) and vehicle-treated mothers.

H-I. Von Kossa/van Gieson staining (H) and H&E staining (I) of clavicles of E18.5 *Runx2+/-* embryos carried by STZ- (150mg/kg) or vehicle-treated mothers.

J. Immunohistochemical detection of Type I and type X collagens in clavicles of E18.5 *Runx2+/-* embryos carried by STZ- (150mg/kg) or vehicle-treated mothers.

K. Runx2 and α1(I)Collagen accumulations in femurs of E18.5 WT and *Runx2+/-* embryos carried by STZ- (150mg/kg) or vehicle-treated mothers.

L. *α1(I)* and *α2(I) Collagen* expression in femurs of E18.5 WT and *Runx2+/−* embryos carried by STZ- (150mg/kg) or vehicle-treated mothers (n=8).

M. Runx2 and α1(I)Collagen accumulations in femurs of E18.5 WT and *Runx2−/−* embryos carried by STZ- (150mg/kg) or vehicle-treated mothers.

N. *Akp2* expression in femurs of E18.5 of WT and *Runx2−/−* embryos carried by STZ- (150mg/kg) or vehicle-treated mothers (n=6).

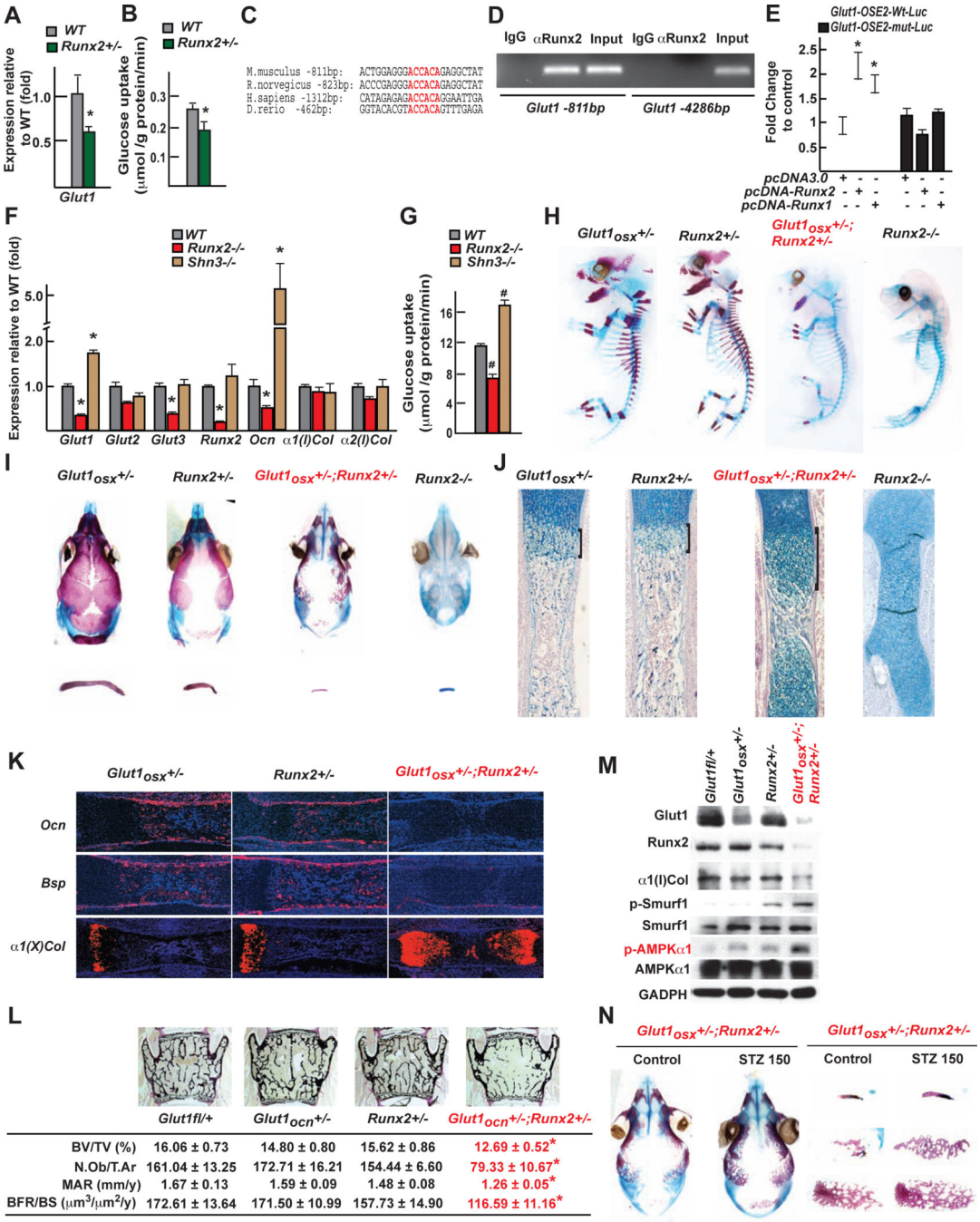

Figure 7. The reciprocal regulation between Runx2 and Glut1 determines osteoblast differentiation and bone formation

A. *Glut1* expression in femurs of 3 month-old *Runx2*+/− mice (n=8).

B. Uptake rate of 2-DG in the calvaria of 6 week-old WT and *Runx2*+/− (n=4-5)mice.

C. Runx binding sites in the *Glut1* promoter of several species.

D. ChIP assay of Runx2 binding to the promoter of mouse *Glut1*.

E. Luciferase assay of *pGlut1*-WT-*Luc* or *pGlut1-mut-Luc* in COS cells cotransfected with Runx2 or Runx1 expression vector (n=6).

F. Expression of osteoblast marker genes in WT, *Runx2−/− and Shn3−/−*osteoblasts (n=6).
G. Glucose uptake in WT, *Runx2−/− and Shn3−/−* osteoblasts measured by the uptake rate of 2-DG (n=6).
H-I. Alcian blue/alizarin red staining of skeletal preparations of E16.5 (H) and 18.5 (I) *Glut1*$_{osx}$*+/−*, *Runx2+/−*, *Glut1*$_{osx}$*+/−;Runx2+/-* and *Runx2−/−* embryos.
J. Alcian blue staining of histological sections of femurs of E18.5 *Glut1*$_{osx}$*+/−*, *Runx2+/−*, *Glut1*$_{osx}$*+/−;Runx2+/−* and *Runx2−/−* embryos.
K. In situ hybridization analysis of *Osteocalcin*, *Bsp* and *α1(X) Collagen* expression, in E18.5 *Glut1*$_{osx}$*+/−*, *Runx2+/−* and *Glut1*$_{osx}$*+/−;Runx2+/−* femurs.
L. Bone histomorphometric analysis of L4 vertebrae of 3 month-old of *Glut1fl/+*, *Glut1*$_{ocn}$*+/−*, *Runx2+/−* and *Glut1*$_{ocn}$*+/−;Runx2+/−* female mice (n=9-12).
M. Runx2 and α1(I)Collagen accumulations and AMPKα1 and Smurf1 phosphorylation in femurs of E18.5 *Glut1fl/+*, *Glut1*$_{osx}$*+/−*, *Runx2+/−*, and *Glut1*$_{osx}$*+/−; Runx2+/−* embryos.
N. Alcian blue/alizarin red staining of skeletal preparations of E18.5 *Glut1*$_{osx}$*+/− ;Runx2+/−* embryos carried by mothers treated with STZ (150mg/kg) or vehicle.